

Supplementary Information for “Ornstein-Uhlenbeck information swimmers with external and internal feedback controls”

Zhanglin Hou,^{1,2} Ziluo Zhang,^{1,3} Jun Li,^{4,1} Kento Yasuda,⁵ and Shigeeyuki Komura^{1,2,6,*}

¹Wenzhou Institute, University of Chinese Academy of Sciences, Wenzhou, Zhejiang 325001, China

²Oujiang Laboratory, Wenzhou, Zhejiang 325000, China

³Institute of Theoretical Physics, Chinese Academy of Sciences, Beijing 100190, China

⁴Department of Physics, Wenzhou University, Wenzhou, Zhejiang 325035, China

⁵Research Institute for Mathematical Sciences, Kyoto University, Kyoto 606-8502, Japan

⁶Department of Chemistry, Graduate School of Science, Tokyo Metropolitan University, Tokyo 192-0397, Japan

I. EFFECTIVE TEMPERATURE OF AN ACTIVE ORNSTEIN-UHLENBECK PARTICLE

The effective temperature of an active Ornstein-Uhlenbeck particle (AOUP) is obtained by using its equal-time velocity correlation function $\langle \tilde{v}^2 \rangle$. Here, we briefly present our mathematical scheme to obtain it, while the details of a similar approach can be found in Refs. [1, 2]. The dimensionless equation of motion for an AOUP can be written as

$$\frac{d\tilde{v}(\tilde{t})}{d\tilde{t}} = -[\tilde{v}(\tilde{t}) - \tilde{u}(\tilde{t})] + \tilde{\zeta}(\tilde{t}), \quad (\text{S1})$$

$$\frac{d\tilde{u}(\tilde{t})}{d\tilde{t}} = -\frac{\tilde{u}(\tilde{t})}{\tilde{\tau}_a} + \frac{\sqrt{\tilde{A}}}{\tilde{\tau}_a} \tilde{\xi}(\tilde{t}), \quad (\text{S2})$$

$$\langle \tilde{\zeta}(\tilde{t}) \rangle = 0, \quad \langle \tilde{\zeta}(\tilde{t}) \tilde{\zeta}(\tilde{t}') \rangle = 2\delta(\tilde{t} - \tilde{t}'), \quad (\text{S3})$$

$$\langle \tilde{\xi}(\tilde{t}) \rangle = 0, \quad \langle \tilde{\xi}(\tilde{t}) \tilde{\xi}(\tilde{t}') \rangle = 2\delta(\tilde{t} - \tilde{t}'). \quad (\text{S4})$$

The above equations can be converted to the following Fokker-Planck equation for the probability distribution function $P(\tilde{v}, \tilde{u}; t)$:

$$\frac{\partial P}{\partial t} = \frac{\partial^2 P}{\partial \tilde{v}^2} + \frac{\partial}{\partial \tilde{v}}[(\tilde{v} - \tilde{u})P] + \frac{\tilde{A}}{\tilde{\tau}_a} \frac{\partial^2 P}{\partial \tilde{u}^2} + \frac{\partial}{\partial \tilde{u}}(\tilde{u}P). \quad (\text{S5})$$

We use the Doi-Peliti field theory to obtain the correlation function. Using the definition $L = \sqrt{\tilde{A}/\tilde{\tau}_a}$, we first introduce the fields as

$$\tilde{\phi}^{(\sim)}(\tilde{v}, t) = \int \frac{d\omega}{2\pi} e^{-i\omega t} \sum_{n=0}^{\infty} \tilde{f}_n^{(\sim)}(\tilde{v}), \quad (\text{S6})$$

$$\tilde{\psi}^{(\sim)}(\tilde{u}, t) = \int \frac{d\omega}{2\pi} e^{-i\omega t} \frac{1}{L} \sum_{n=0}^{\infty} \tilde{f}_n^{(\sim)}(\tilde{u}/L), \quad (\text{S7})$$

where ϕ and ψ are the annihilation fields, whereas $\tilde{\phi}$ and $\tilde{\psi}$ are the Doi-shifted creation fields [1, 2]. The functions $\tilde{f}_n^{(\sim)}$ are defined as

$$f_n(x) = e^{-x^2/2} He_n(x), \quad (\text{S8})$$

$$\tilde{f}_n(x) = \frac{1}{\sqrt{2\pi n!}} He_n(x), \quad (\text{S9})$$

where $He_n(x)$ is the n -th order of the probabilist's Hermite polynomial [1, 2]. Their orthogonality relation is given by

$$\int dx f_n(x/L) \tilde{f}_m(x/L) = L\delta_{nm}, \quad (\text{S10})$$

* Corresponding author: komura@wiucas.ac.cn

where δ_{nm} is the Kronecker delta and $f_n(x/L)$ is the eigenfunction of the following operator:

$$L^2 \partial_x^2 f_n(x/L) + \partial_x [x f_n(x/L)] = -n f_n(x/L). \quad (\text{S11})$$

The two-point correlation function under the given initial state $(\tilde{v}_0, \tilde{u}_0, t_0)$ is written as

$$P(\tilde{v}, \tilde{u}, t | \tilde{v}_0, \tilde{u}_0, t_0) = \langle \phi(\tilde{v}, t) \psi(\tilde{u}, t) \tilde{\phi}(\tilde{v}_0, t_0) \tilde{\psi}(\tilde{u}_0, t_0) \rangle \quad (\text{S12})$$

$$= \frac{1}{L^2} \sum_{n, n', m, m'} f_n(\tilde{v}) f_m(\tilde{u}/L) \langle \phi_n(t) \psi_m(t) \tilde{\phi}_{n'}(t_0) \tilde{\psi}_{m'}(t_0) \rangle \tilde{f}_{n'}(\tilde{v}) \tilde{f}_{m'}(\tilde{u}/L). \quad (\text{S13})$$

Then, the equal-time correlation function is calculated by

$$\langle \tilde{v}^2 \rangle = \lim_{t_0 \rightarrow -\infty} \int d\tilde{v} \int d\tilde{u} \tilde{v}^2 P(\tilde{v}, \tilde{u}, t | \tilde{v}_0, \tilde{u}_0, t_0). \quad (\text{S14})$$

We substitute Eq. (S13) into Eq. (S14) and use the relation $x^2 = He_2(x) + He_0(x)$. Applying the orthogonality conditions of the Hermite polynomials, we finally obtain the equal-time correlation as

$$\langle \tilde{v}^2 \rangle = 1 + \frac{\tilde{A}}{1 + \tilde{\tau}_a}. \quad (\text{S15})$$

Here, the second term corresponds to the temperature increase due to the Ornstein-Uhlenbeck noise.

II. ADDITIONAL NUMERICAL DATA

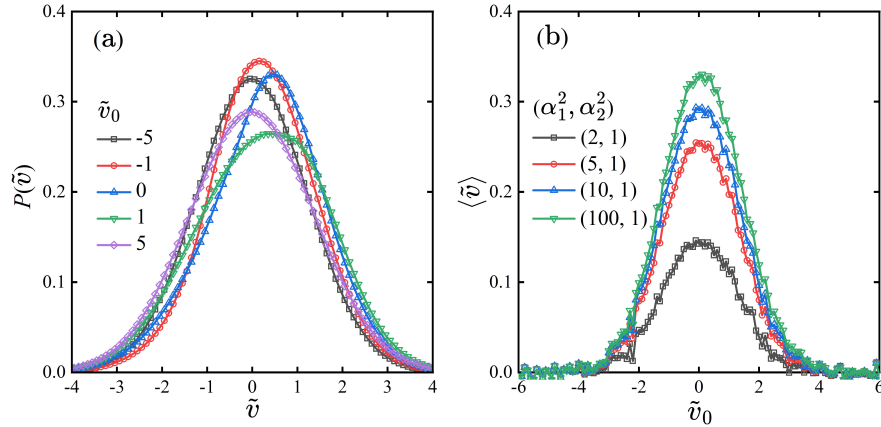


FIG. S1. Various statistical properties of the E-OUIS model with external feedback control [see Eqs. (5)–(8)]. The fixed parameters are $\tilde{\tau}_a = 1$, $\tilde{A} = 1$, and $\tilde{\tau}_m = 1$. (a) The steady-state velocity distribution function $P(\tilde{v})$ when the threshold velocity is changed within the range of $-5 \leq v_0 \leq 5$. Here, we choose $(\alpha_1^2, \alpha_2^2) = (10, 1)$. (b) The steady-state average velocity $\langle \tilde{v} \rangle$ as a function of the threshold velocity \tilde{v}_0 when $(\alpha_1^2, \alpha_2^2) = (2, 1), (5, 1), (10, 1)$ and $(100, 1)$.

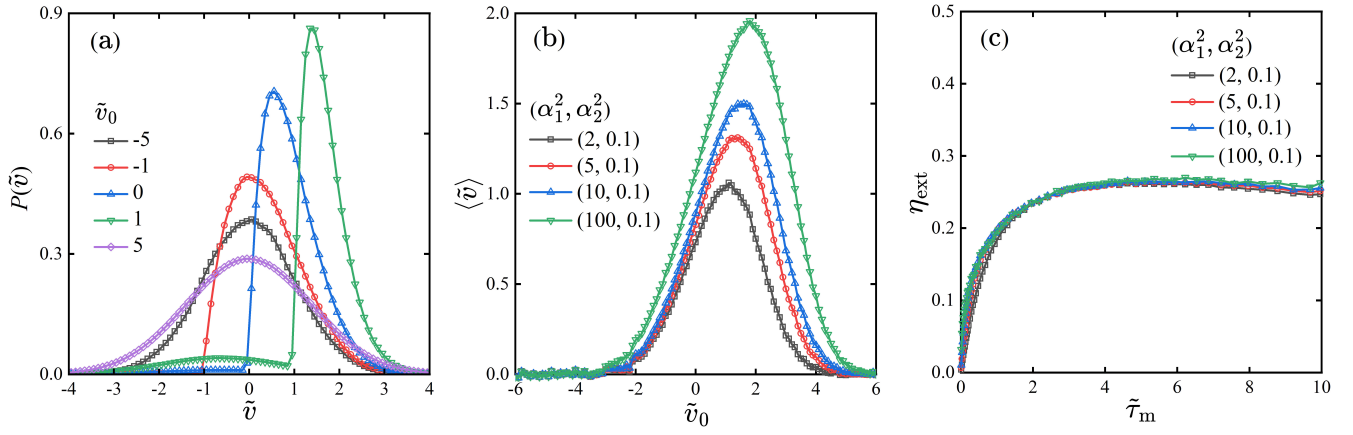


FIG. S2. Various statistical properties of the E-OUIS model with external feedback control [see Eqs. (5)–(8)]. The fixed parameters are $\tilde{\tau}_a = 1$ and $\tilde{A} = 1$. (a) The steady-state velocity distribution function $P(\tilde{v})$ when the threshold velocity is changed within the range of $-5 \leq v_0 \leq 5$. Here, we choose $(\alpha_1^2, \alpha_2^2) = (10, 0.1)$ and the measurement time interval is $\tilde{\tau}_m = 0.01$. (b) The steady-state average velocity $\langle \tilde{v} \rangle$ as a function of the threshold velocity \tilde{v}_0 when $(\alpha_1^2, \alpha_2^2) = (2, 0.1)$, $(5, 0.1)$, $(10, 0.1)$, $(100, 0.1)$ and $\tilde{\tau}_m = 0.01$. (c) The efficiency η_{ext} of the E-OUIS model with external feedback control [see Eq. (10)] as a function of $\tilde{\tau}_m$ for the same combinations of (α_1^2, α_2^2) shown in (b). The threshold velocity is $\tilde{v}_0 = 0$.

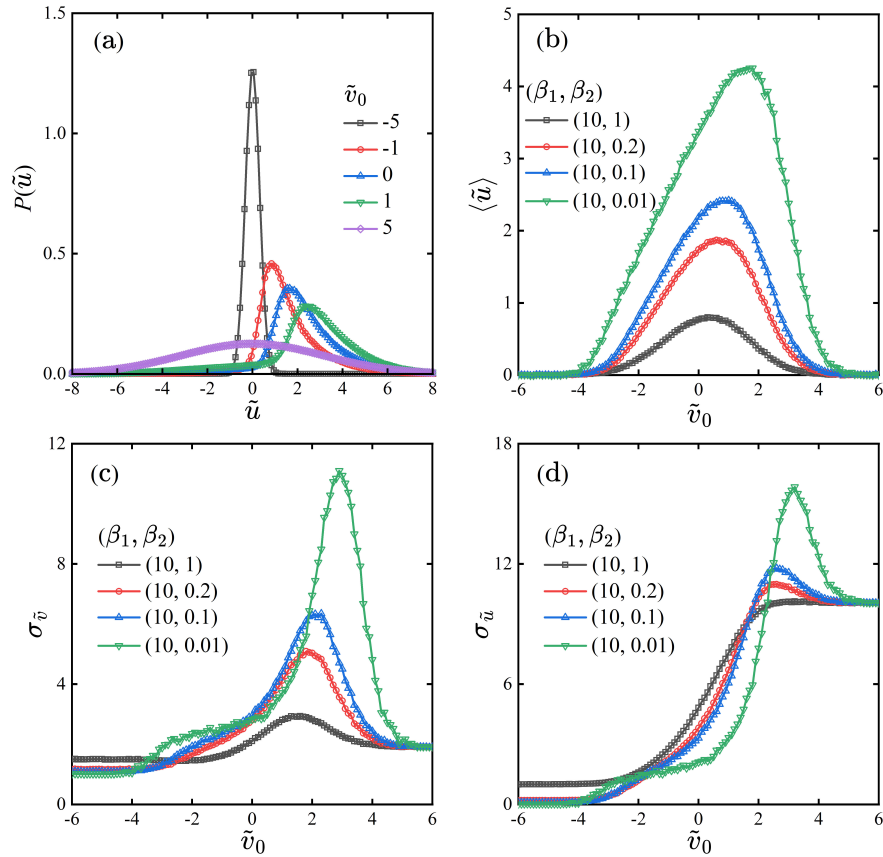


FIG. S3. Various statistical properties of the I-OUIS model with internal feedback control [see Eqs. (13)–(16)]. The fixed parameters are $\tilde{\tau}_a = 1$, $\tilde{A} = 1$, and $\tilde{\tau}_m = 0.01$. (a) The steady-state self-propulsion velocity distribution function $P(\tilde{u})$ when the threshold velocity is changed within the range of $-5 \leq v_0 \leq 5$. Here, we choose $(\beta_1, \beta_2) = (10, 0.1)$. (b) The steady-state average self-propulsion velocity $\langle \tilde{u} \rangle$ as a function of the threshold velocity \tilde{v}_0 when $(\beta_1, \beta_2) = (10, 1)$, $(10, 0.2)$, $(10, 0.1)$ and $(10, 0.01)$. (c) The variance $\sigma_{\tilde{v}}$ of the steady-state velocity distribution function $P(\tilde{v})$ in Fig. 2 as a function of \tilde{v}_0 . (d) The variance $\sigma_{\tilde{u}}$ of the steady-state self-propulsion velocity distribution function $P(\tilde{u})$ in Fig. S3 as a function of \tilde{v}_0 .

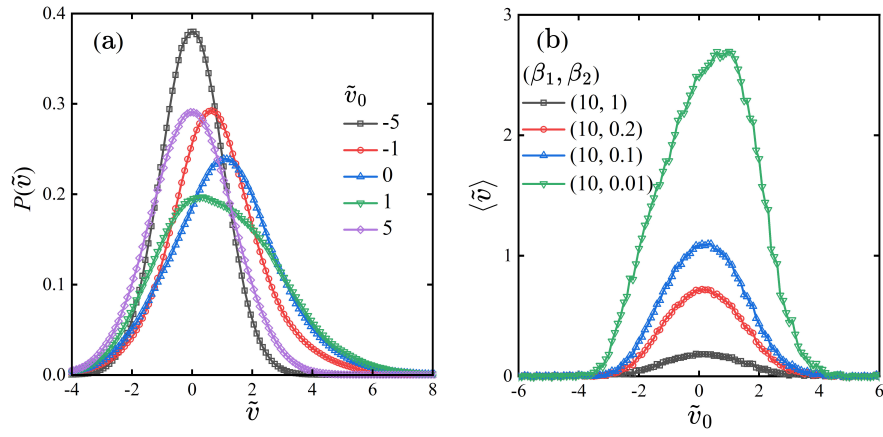


FIG. S4. Various statistical properties of the I-OUIS model with internal feedback control [see Eqs. (13)–(16)]. The fixed parameters are $\tilde{\tau}_a = 1$, $\tilde{A} = 1$, and $\tilde{\tau}_m = 1$. (a) The steady-state velocity distribution function $P(\tilde{v})$ when the threshold velocity is changed within the range of $-5 \leq v_0 \leq 5$. Here, we choose $(\beta_1, \beta_2) = (10, 0.1)$. (b) The steady-state average velocity $\langle \tilde{v} \rangle$ as a function of the threshold velocity \tilde{v}_0 when $(\beta_1, \beta_2) = (10, 1)$, $(10, 0.2)$, $(10, 0.1)$ and $(10, 0.01)$.

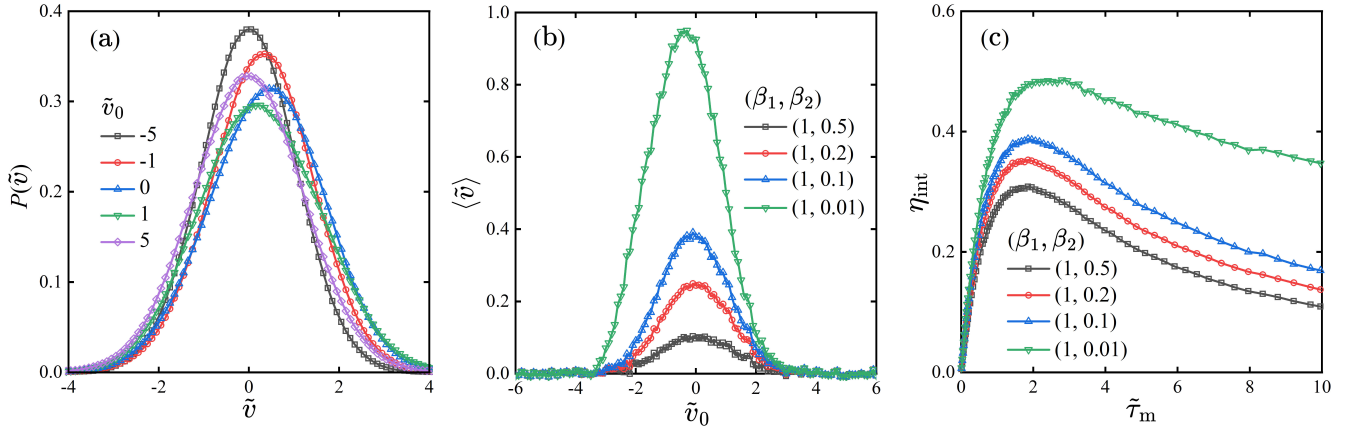


FIG. S5. Various statistical properties of the I-OUIS model with internal feedback control [see Eqs. (13)–(16)]. The fixed parameters are $\tilde{\tau}_a = 1$ and $\tilde{A} = 1$. (a) The steady-state velocity distribution function $P(\tilde{v})$ when the threshold velocity is changed within the range of $-5 \leq v_0 \leq 5$. Here, we choose $(\beta_1, \beta_2) = (1, 0.1)$ and the measurement time interval is $\tilde{\tau}_m = 0.01$. (b) The steady-state average velocity $\langle \tilde{v} \rangle$ as a function of the threshold velocity \tilde{v}_0 when $(\beta_1, \beta_2) = (1, 0.5)$, $(1, 0.2)$, $(1, 0.1)$, $(1, 0.01)$ and $\tilde{\tau}_m = 0.01$. (c) The efficiency η_{int} of the I-OUIS model with internal feedback control [see Eq. (17)] as a function of $\tilde{\tau}_m$ for the same combinations of (β_1, β_2) shown in (b). The threshold velocity is $\tilde{v}_0 = 0$.

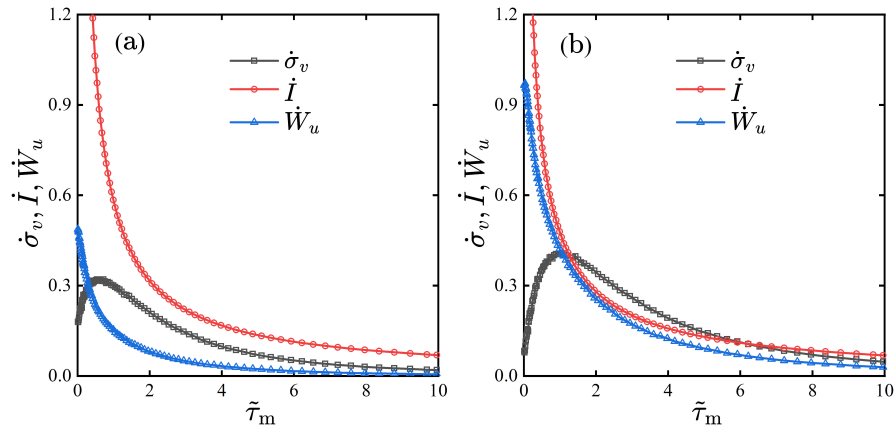


FIG. S6. Contributions of dimensionless $\dot{\sigma}_v$, \dot{I} , and \dot{W}_u to the efficiency η_{int} of the I-OUIS model [see Eq. (17)] as a function of $\tilde{\tau}_m$. The choice of parameters corresponds to that of (a) $\tilde{A} = 1$ (red) and (b) $\tilde{A} = 5$ (green) in Fig. 3(c).

-
- [1] R. Garcia-Millan and G. Pruessner, Run-and-tumble motion in a harmonic potential: field theory and entropy production, *J. Stat. Mech.*, 063203 (2021).
 - [2] Z. Zhang, S. Yuan, and S. Komura, Field theory of active Brownian particles with dry friction, *New J. Phys.* 26, 093036 (2024).

Ornstein-Uhlenbeck information swimmers with external and internal feedback controls

Zhanglin Hou,^{1,2} Ziluo Zhang,^{1,3} Jun Li,^{4,1} Kento Yasuda,⁵ and Shigeyuki Komura^{1,2,6,*}

¹Wenzhou Institute, University of Chinese Academy of Sciences, Wenzhou, Zhejiang 325001, China

²Oujiang Laboratory, Wenzhou, Zhejiang 325000, China

³Institute of Theoretical Physics, Chinese Academy of Sciences, Beijing 100190, China

⁴Department of Physics, Wenzhou University, Wenzhou, Zhejiang 325035, China

⁵Research Institute for Mathematical Sciences, Kyoto University, Kyoto 606-8502, Japan

⁶Department of Chemistry, Graduate School of Science,
Tokyo Metropolitan University, Tokyo 192-0397, Japan

Using an underdamped active Ornstein-Uhlenbeck particle, we propose two information swimmer models having either external or internal feedback control and perform their numerical simulations. Depending on the velocity that is measured after every fixed time interval (measurement time), the friction coefficient is modified in the externally controlled model, whereas the persistence time for the activity is changed in the internally controlled one. In the steady state, both of these information swimmers acquire finite average velocities in the noisy environment, and the efficiency can be maximized by tuning the measurement time. The internally controlled swimmer is more relevant to biological systems and can generally achieve larger average velocity and efficiency than the externally controlled model.

Introduction.— In the studies of active matter, much interest has been focused on the collective motion of self-propelled particles [1]. On the other hand, it is also important to understand the mechanism of single-particle motion from the perspective of non-equilibrium statistical mechanics [2]. Among various models, the self-propulsion of an active Brownian particle (ABP) is generated by an internal driving force combined with overdamped orientational Brownian dynamics [3]. An overdamped fluctuating self-propelled motion in a viscous fluid can be described by an active Ornstein-Uhlenbeck particle (AOUP) [4] driven by a stochastic force whose memory decays exponentially in time. Since the AOUP model exhibits persistent particle motion mimicking the activity, it offers a basic reference for active dynamics of cells and bacteria [5].

Although both ABP and AOUP are active particles, they undergo Brownian dynamics in the long time limit [6] and cannot have any net locomotion on average. For microswimmers in a Newtonian fluid, it is known that non-reciprocal cyclic body motion is required for their persistent locomotion [7, 8]. To maintain such continuous movement, a constant supply of mechanical energy and its dissipation to the surrounding fluid should take place [9]. Other active systems driven by mechanical work include Janus particles that consume a chemical fuel [10]. In contrast to these microswimmers, the “odd microswimmer” consisting of three spheres and two odd springs is purely driven by the thermal energy of the surrounding fluid [11, 12].

Recently, much attention has been paid to active systems that utilize information instead of energy, i.e., informational active matter [13]. During the last decade, there have been many studies on “information engines” that use information to extract mechanical work [14–16]. One example of such an engine proposed by Huang *et al.* is the model of “information swimmer” in which the swimmer periodically measures its velocity and adjusts its friction coefficient [17]. They

showed that the information swimmer can achieve a steady-state velocity without external energy input although it does not violate the extended second law of thermodynamics with information [18]. Such an information swimmer can also be regarded as one type of “information ratchet” that leads to directional transport or locomotion by repeating measurements and feedback control [19, 20].

In the absence of measurement and feedback, the information swimmer proposed by Huang *et al.* [17] is passive and purely governed by thermal fluctuations. From the viewpoint of informational active matter [13], it is of interest to consider an information swimmer that controls its internal activity depending on the result of the measurement. In this Letter, we propose models of information swimmers by using an underdamped AOUP and call them “Ornstein-Uhlenbeck information swimmers” (OUIs). To highlight the role of activity, we discuss two different information swimmers: (i) OUIS with *external* feedback control (E-OUIS) and (ii) OUIS with *internal* feedback control (I-OUIS). Depending on the particle velocity, the friction coefficient is adjusted in the E-OUIS (similar to Ref. [17]), whereas the persistence time for the activity is controlled in the I-OUIS. The latter I-OUIS model is more relevant to biological systems [21], such as the run-and-tumble motion of *Escherichia coli* [22, 23]. We perform numerical simulations of the two models and discuss their swimming performance. Although both OUIS models can maintain a steady motion along the chosen direction, the efficiency of the I-OUIS can be higher than that of the E-OUIS.

OUIS with external feedback control (E-OUIS).— We consider an underdamped AOUP moving in a one-dimensional space [24, 25]. In the E-OUIS model, the AOUP measures its velocity v after every time interval τ_m and compares it with a threshold velocity v_0 [17, 26]. The friction coefficient is set to $\alpha_1^2\Gamma$ and $\alpha_2^2\Gamma$ if $v \leq v_0$ and $v > v_0$, respectively, where α_1 and α_2 are dimensionless coefficients and we typically choose $\alpha_1 > \alpha_2$. The change in the friction coefficient can be induced such as by that of the particle volume, shape, or surface structure. The results of measurement are recorded in the swimmer’s internal memory, which is assumed to be sufficiently

* Corresponding author: komura@wiucas.ac.cn

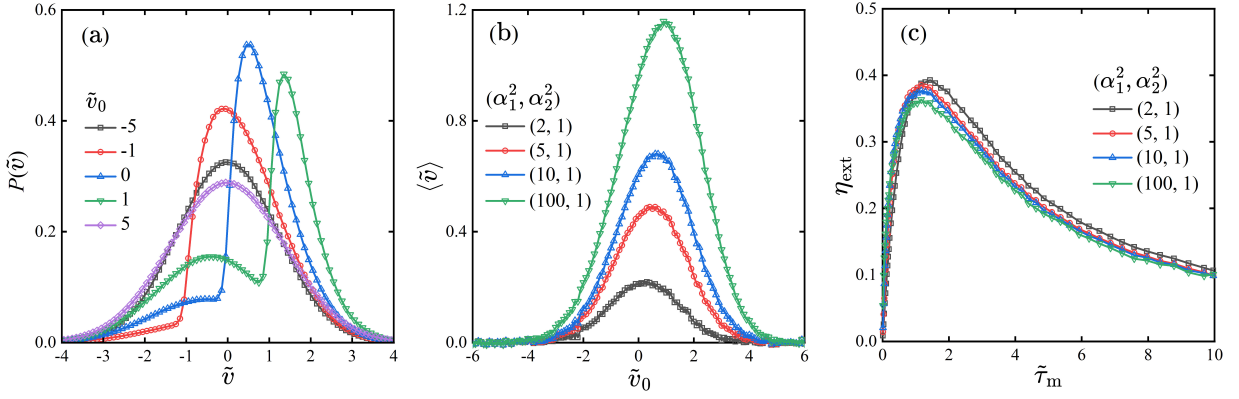


FIG. 1. Various statistical properties of the E-OUIS model with external feedback control [see Eqs. (5)–(8)]. The fixed parameters are $\tilde{\tau}_a = 1$ and $\tilde{A} = 1$. (a) The steady-state velocity distribution function $P(\tilde{v})$ when the threshold velocity is changed within the range of $-5 \leq v_0 \leq 5$. Here, we choose $(\alpha_1^2, \alpha_2^2) = (10, 1)$ and the measurement time interval is $\tilde{\tau}_m = 0.01$. (b) The steady-state average velocity $\langle \tilde{v} \rangle$ as a function of the threshold velocity \tilde{v}_0 when $(\alpha_1^2, \alpha_2^2) = (2, 1), (5, 1), (10, 1), (100, 1)$ and $\tilde{\tau}_m = 0.01$. (c) The efficiency η_{ext} of the E-OUIS model [see Eq. (10)] as a function of $\tilde{\tau}_m$ for the same combinations of (α_1^2, α_2^2) shown in (b). The threshold velocity is $\tilde{v}_0 = 0$.

large.

During the time interval $n\tau_m < t < (n+1)\tau_m$, the Langevin equation for the underdamped E-OUIS is given by

$$M\dot{v}(t) = \begin{cases} -\alpha_1^2\Gamma[v(t) - u(t)] + \alpha_1\sqrt{2\Gamma T}\zeta(t), & v(n\tau_m) \leq v_0, \\ -\alpha_2^2\Gamma[v(t) - u(t)] + \alpha_2\sqrt{2\Gamma T}\zeta(t), & v(n\tau_m) > v_0. \end{cases} \quad (1)$$

Here, $\dot{v} = dv/dt$, M is the particle mass, Γ is the friction coefficient, T is the temperature (we set the Boltzmann constant to be unity, $k_B = 1$), and $\zeta(t)$ is the Gaussian white noise with zero mean and unit variance:

$$\langle \zeta(t) \rangle = 0, \quad \langle \zeta(t)\zeta(t') \rangle = \delta(t - t'). \quad (2)$$

The coefficients of the noise terms in Eq. (1) are chosen to satisfy the fluctuation-dissipation relation for both $v \leq v_0$ and $v > v_0$, reflecting the equilibrium nature of the ambient environment [27]. Note that the threshold velocity v_0 can take both positive and negative values.

In Eq. (1), the velocity u describes the self-propulsion of the particle and it evolves through an Ornstein-Uhlenbeck process [4]

$$\dot{u}(t) = -\frac{u(t)}{\tau_a} + \frac{\sqrt{2A}}{\tau_a}\xi(t), \quad (3)$$

where τ_a is the persistence time, A is the strength of active fluctuation (having the dimension of a diffusion constant). The term $\xi(t)$ in Eq. (3) also represents the Gaussian white noise with zero mean and unit variance:

$$\langle \xi(t) \rangle = 0, \quad \langle \xi(t)\xi(t') \rangle = \delta(t - t'). \quad (4)$$

The parameters τ_a and A can be used to quantify the activity of the AOUP, such as the persistence length $\ell_0 = \sqrt{A\tau_a}$ and the magnitude of the self-propulsion velocity $u_0 = \sqrt{A/\tau_a}$ [24, 25].

In the following analysis, we use the Brownian relaxation time $\tau = M/\Gamma$ and the thermal velocity $v_T = \sqrt{T/M}$ to rescale

all the variables as $\tilde{t} = t/\tau$, $\tilde{v}(\tilde{t}) = v(t)/v_T$, $\tilde{u}(\tilde{t}) = u(t)/v_T$, $\tilde{\zeta}(\tilde{t}) = \sqrt{2M/\Gamma}\zeta(t)$, and $\tilde{\xi}(\tilde{t}) = \sqrt{2M/\Gamma}\xi(t)$. Moreover, the dimensionless model parameters are defined as $\tilde{\tau}_m = \tau_m/\tau$, $\tilde{v}_0 = v_0/v_T$, $\tilde{\tau}_a = \tau_a/\tau$, and $\tilde{A} = A\Gamma/T$. Then, the dimensionless form of the E-OUIS model can be summarized as

$$\frac{d\tilde{v}(\tilde{t})}{d\tilde{t}} = \begin{cases} -\alpha_1^2[\tilde{v}(\tilde{t}) - \tilde{u}(\tilde{t})] + \alpha_1\tilde{\zeta}(\tilde{t}), & \tilde{v}(n\tilde{\tau}_m) \leq \tilde{v}_0, \\ -\alpha_2^2[\tilde{v}(\tilde{t}) - \tilde{u}(\tilde{t})] + \alpha_2\tilde{\zeta}(\tilde{t}), & \tilde{v}(n\tilde{\tau}_m) > \tilde{v}_0, \end{cases} \quad (5)$$

$$\frac{d\tilde{u}(\tilde{t})}{d\tilde{t}} = -\frac{\tilde{u}(\tilde{t})}{\tilde{\tau}_a} + \frac{\sqrt{\tilde{A}}}{\tilde{\tau}_a}\tilde{\xi}(\tilde{t}), \quad (6)$$

$$\langle \tilde{\zeta}(\tilde{t}) \rangle = 0, \quad \langle \tilde{\zeta}(\tilde{t})\tilde{\zeta}(\tilde{t}') \rangle = 2\delta(\tilde{t} - \tilde{t}'), \quad (7)$$

$$\langle \tilde{\xi}(\tilde{t}) \rangle = 0, \quad \langle \tilde{\xi}(\tilde{t})\tilde{\xi}(\tilde{t}') \rangle = 2\delta(\tilde{t} - \tilde{t}'), \quad (8)$$

for $n\tilde{\tau}_m < \tilde{t} < (n+1)\tilde{\tau}_m$.

When $\alpha_1 = \alpha_2 = 1$, namely, when measurement and feedback control are absent, one can easily convert the above Langevin equations to a Fokker-Planck equation and obtain the velocity autocorrelation function of an ordinary AOUP, as explained in the Supplementary Information (SI). Using the equal-time velocity correlation, one can define the effective temperature of an AOUP as $T^* = M\langle v^2 \rangle$, where

$$T^* = T + \frac{A\Gamma\tau}{\tau + \tau_a} = T \left(1 + \frac{\tilde{A}}{1 + \tilde{\tau}_a} \right). \quad (9)$$

Hence, the effective temperature satisfies $T^* > T$, and the additional term is proportional to the active fluctuation strength A . Hereafter, we use the dimensionless effective temperature $\tilde{T}^* = T^*/T$. When $\alpha_1 = \alpha_2$, however, the E-OUIS does not exhibit any net locomotion in the long time limit, as mentioned before.

The above stochastic equations for the E-OUIS are discretized over the small time step $\Delta\tilde{t} = 0.001$, and they are numerically integrated by using the first-order Euler-Maruyama scheme [28]. Among several model parameters, we fix $\tilde{\tau}_a = 1$ and $\tilde{A} = 1$, but change α_1^2 , α_2^2 , $\tilde{\tau}_m$, and \tilde{v}_0 . When the particle has reached the steady state after 10^7 time steps, we obtain the

time-independent velocity distribution function $P(\tilde{v})$ to calculate the steady-state average velocity $\langle \tilde{v} \rangle = \int_{-\infty}^{\infty} d\tilde{v} \tilde{v} P(\tilde{v})$. In the E-OUIS model, however, the steady-state distribution function $P(\tilde{u})$ of the self-propulsion velocity u is purely Gaussian [see Eqs. (6) and (8)], and its average should vanish, $\langle \tilde{u} \rangle = 0$.

In Fig. 1(a), we show the results of the steady-state velocity distribution function $P(\tilde{v})$ of the E-OUIS when $(\alpha_1^2, \alpha_2^2, \tilde{\tau}_m) = (10, 1, 0.01)$ (corresponding to $\tilde{\tau}_m = 10\Delta\tilde{t}$) and \tilde{v}_0 is varied between $-5 \leq \tilde{v}_0 \leq 5$. When the absolute value of the threshold velocity is as large as $|\tilde{v}_0| \approx 5$, the distribution function $P(\tilde{v})$ is almost Gaussian and the average velocity $\langle \tilde{v} \rangle$ vanishes. For $|\tilde{v}_0| < 4$, however, $P(\tilde{v})$ becomes highly asymmetric and even bimodal for $\tilde{v}_0 > 0$. In such a situation, the steady-state average velocity is finite, $\langle \tilde{v} \rangle > 0$, and hence the E-OUIS model acquires net locomotion under the noisy stochastic environment. Since we assume that the change of the friction coefficient does not require any mechanical work [17], the E-OUIS model is purely driven by measurement and feedback control. In Fig. 1(b), we plot the average velocity $\langle \tilde{v} \rangle$ as a function of the threshold velocity \tilde{v}_0 for different values of α_1^2 . The maximum of $\langle \tilde{v} \rangle$ becomes larger for larger α_1^2 , and it occurs at positive \tilde{v}_0 such as at $\tilde{v}_0 \approx 0.6$ when $\alpha_1^2 = 10$. The induced average velocity is the order of thermal velocity v_T .

Next, we argue the swimming performance of the E-OUIS model. First, the change rate of information entropy is given by $\dot{I} = I/\tau_m$, where I is the mutual information [18]. Since there is no error in the measurement, the mutual information is equal to the Shannon entropy, $I = -\sum_i p_i \ln p_i$, where p_i is the probability of the state $i = 1, 2$ and satisfies $\sum_i p_i = 1$. The entropy production rate due to the frictional motion can be estimated by $\dot{\sigma}_v = \sum_i \alpha_i^2 \Gamma \langle v - u \rangle_i \langle v \rangle_i p_i / T^*$, where T^* is the effective temperature introduced in Eq. (9) (the dimension of $\dot{\sigma}_v$ is inverse time). Then, we define the entropic efficiency of the E-OUIS model as

$$\eta_{\text{ext}} = \frac{\dot{\sigma}_v}{\dot{I}} = \frac{\sum_i \alpha_i^2 \langle \tilde{v} - \tilde{u} \rangle_i \langle \tilde{v} \rangle_i p_i / \tilde{T}^*}{I / \tilde{\tau}_m}. \quad (10)$$

The above efficiency η_{ext} is plotted as a function of the measurement time $\tilde{\tau}_m$ in Fig. 1(c) when $\tilde{v}_0 = 0$. The overall behavior is similar for different choices of α_1^2 . The efficiency is low for small and large $\tilde{\tau}_m$ values, taking a maximum value $\eta_{\text{ext}} \approx 0.38$ at around $\tilde{\tau}_m \approx 1$ for all α_1^2 . In other words, the efficiency is maximized when the measurement time τ_m is close to the Brownian relaxation time τ . As separately shown in Fig. S1 of the SI, the velocity distribution function $P(\tilde{v})$ for $\tilde{\tau}_m = 1$ is more symmetric and $\langle \tilde{v} \rangle$ is smaller than that for $\tilde{\tau}_m = 0.01$. However, since \dot{I} becomes also smaller due to the larger measurement time $\tau_m = 1$, the efficiency η_{ext} can still be maximized at around $\tilde{\tau}_m \approx 1$. We have further checked the other cases of $(\alpha_2^2, \tilde{\tau}_m) = (0.1, 0.01)$ and systematically changed α_1^2 , as shown in Fig. S2. The results are similar to those in Fig. 1, showing a robust dependence on the model parameters. However, the efficiency η_{ext} decreases much slower when τ_m is made larger, as shown in Fig. S2(c).

OUIS with internal feedback control (I-OUIS).— In the previous E-OUIS model, the friction coefficient of the AOUP was changed according to the measurement of its velocity [see

Eq. (1)]. Next, we consider a different type of OUIS that can change the self-propulsion dynamics of u depending on the velocity v , i.e., OUIS with internal feedback control (I-OUIS). With the same notation as before, the underdamped equation for an AOUP without any external feedback control is given by

$$M\dot{v}(t) = -\Gamma[v(t) - u(t)] + \sqrt{2\Gamma T}\zeta(t), \quad (11)$$

where the Gaussian white noise $\zeta(t)$ satisfies the same statistical properties as in Eq. (2). In the I-OUIS model, the self-propulsion velocity u obeys either of the following equations depending on the measured velocity v after every time interval τ_m

$$\dot{u}(t) = \begin{cases} -\frac{\beta_1 u(t)}{\tau_a} + \frac{\beta_1 \sqrt{2A}}{\tau_a} \xi(t), & v(n\tau_m) \leq v_0, \\ -\frac{\beta_2 u(t)}{\tau_a} + \frac{\beta_2 \sqrt{2A}}{\tau_a} \xi(t), & v(n\tau_m) > v_0, \end{cases} \quad (12)$$

where β_1 and β_2 are dimensionless coefficients and $\xi(t)$ also represents the Gaussian white noise as in Eq. (4). We consider that different values for β_1 and β_2 (typically chosen as $\beta_1 > \beta_2$) give rise to the internal feedback control of the OUIS. Then, the dimensionless form of the I-OUIS model can be summarized as

$$\frac{d\tilde{v}(\tilde{t})}{d\tilde{t}} = -[\tilde{v}(\tilde{t}) - \tilde{u}(\tilde{t})] + \tilde{\zeta}(\tilde{t}), \quad (13)$$

$$\frac{d\tilde{u}(\tilde{t})}{d\tilde{t}} = \begin{cases} -\frac{\beta_1 \tilde{u}(\tilde{t})}{\tilde{\tau}_a} + \frac{\beta_1 \sqrt{\tilde{A}}}{\tilde{\tau}_a} \tilde{\xi}(\tilde{t}), & \tilde{v}(n\tilde{\tau}_m) \leq \tilde{v}_0, \\ -\frac{\beta_2 \tilde{u}(\tilde{t})}{\tilde{\tau}_a} + \frac{\beta_2 \sqrt{\tilde{A}}}{\tilde{\tau}_a} \tilde{\xi}(\tilde{t}), & \tilde{v}(n\tilde{\tau}_m) > \tilde{v}_0, \end{cases} \quad (14)$$

$$\langle \tilde{\zeta}(\tilde{t}) \rangle = 0, \quad \langle \tilde{\zeta}(\tilde{t}) \tilde{\zeta}(\tilde{t}') \rangle = 2\delta(\tilde{t} - \tilde{t}'), \quad (15)$$

$$\langle \tilde{\xi}(\tilde{t}) \rangle = 0, \quad \langle \tilde{\xi}(\tilde{t}) \tilde{\xi}(\tilde{t}') \rangle = 2\delta(\tilde{t} - \tilde{t}'). \quad (16)$$

In Figs. 2(a) and (b), we plot the steady-state velocity distribution function $P(\tilde{v})$ and the average velocity $\langle \tilde{v} \rangle$ of the I-OUIS model, respectively, when $(\beta_1, \beta_2, \tilde{\tau}_m) = (10, 0.1, 0.01)$ for different values of \tilde{v}_0 . Similar to the E-OUIS model, the distribution function $P(\tilde{v})$ becomes asymmetric with the internal feedback control, and the average velocity $\langle \tilde{v} \rangle$ becomes finite. Compared to Fig. 1(b), however, $\langle \tilde{v} \rangle$ is much larger when β_2 is made smaller, and reaches up to $\langle \tilde{v} \rangle \approx 4$ when $(\beta_1, \beta_2) = (10, 0.01)$ as \tilde{v}_0 is varied. Moreover, in contrast to the E-OUIS case, the steady-state distribution function $P(\tilde{u})$ of the self-propulsion velocity u is no longer Gaussian and becomes highly asymmetric, as shown in Fig. S3(a). Even though $P(\tilde{v})$ and $P(\tilde{u})$ are very different in the steady state, we have numerically confirmed that the corresponding average velocities coincide, $\langle \tilde{v} \rangle = \langle \tilde{u} \rangle$, for the I-OUIS model [see Fig. 2(b) and Fig. S3(b)], as can be expected from Eqs. (11) and (13). Notice, however, that the variances of $P(\tilde{v})$ and $P(\tilde{u})$ plotted in Figs. S3(c) and (d), respectively, are apparently different. The results of $P(\tilde{v})$ and $\langle \tilde{v} \rangle$ with a larger measurement time $\tilde{\tau}_m = 1$ for the I-OUIS model are shown in Figs. S4(a) and (b), respectively.

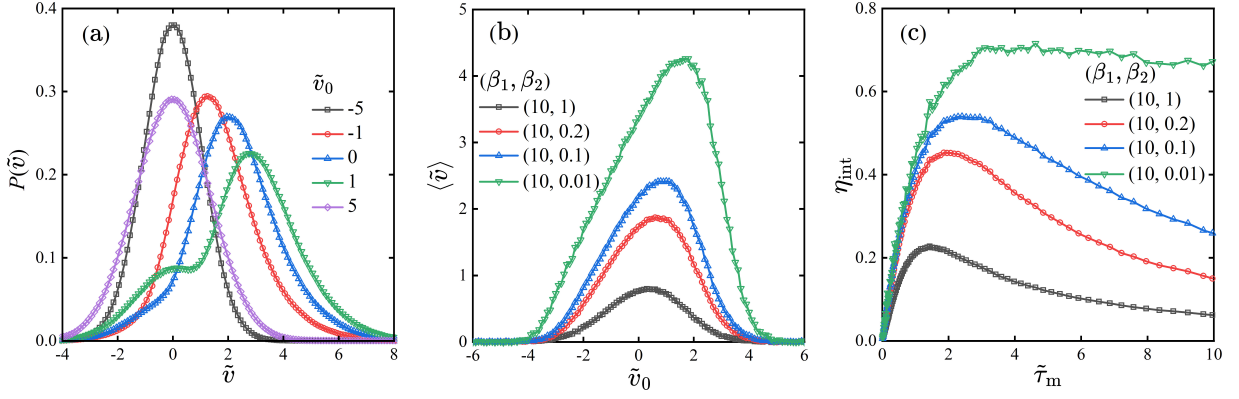


FIG. 2. Various statistical properties of the I-OUIS model with internal feedback control [see Eqs. (13)–(16)]. The fixed parameters are $\tilde{\tau}_a = 1$ and $\tilde{A} = 1$. (a) The steady-state velocity distribution function $P(\tilde{v})$ when the threshold velocity is changed within the range of $-5 \leq v_0 \leq 5$. Here, we choose $(\beta_1, \beta_2) = (10, 0.1)$ and the measurement time interval is $\tilde{\tau}_m = 0.01$. (b) The steady-state average velocity $\langle \tilde{v} \rangle$ as a function of the threshold velocity \tilde{v}_0 when $(\beta_1, \beta_2) = (10, 1), (10, 0.2), (10, 0.1), (10, 0.01)$ and $\tilde{\tau}_m = 0.01$. (c) The efficiency η_{int} of the I-OUIS model [see Eq. (17)] as a function of $\tilde{\tau}_m$ for the same combinations of (β_1, β_2) shown in (b). The threshold velocity is $\tilde{v}_0 = 0$.

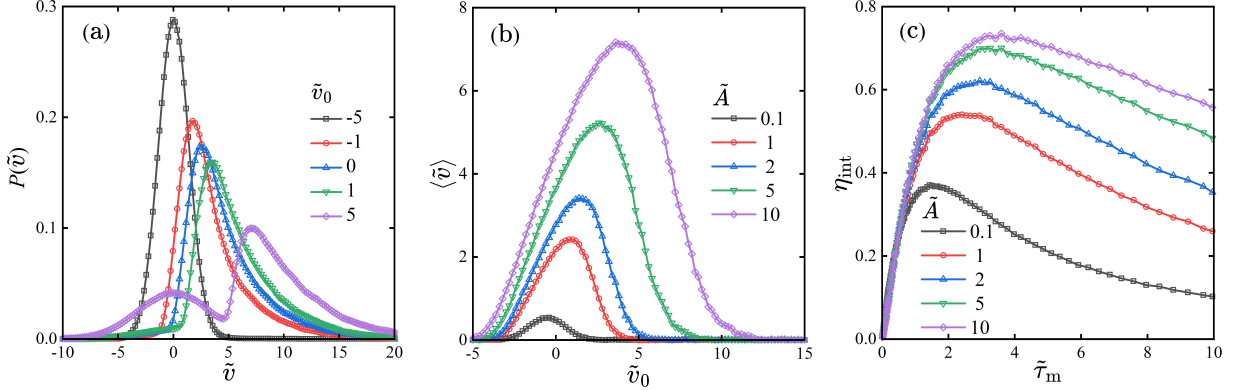


FIG. 3. Various statistical properties of the I-OUIS model with internal feedback control [see Eqs. (13)–(16)]. The fixed parameters are $\tilde{\tau}_a = 1$ and $(\beta_1, \beta_2) = (10, 0.1)$. (a) The steady-state velocity distribution function $P(\tilde{v})$ when the threshold velocity is changed within the range of $-5 \leq v_0 \leq 5$. Here, we choose $\tilde{A} = 10$ and the measurement time interval is $\tilde{\tau}_m = 0.01$. (b) The steady-state average velocity $\langle \tilde{v} \rangle$ as a function of the threshold velocity \tilde{v}_0 when $\tilde{A} = 0.1, 1, 2, 5, 10$ and $\tilde{\tau}_m = 0.01$. (c) The efficiency η_{int} of the I-OUIS model [see Eq. (17)] as a function of $\tilde{\tau}_m$ for the same values of \tilde{A} shown in (b). The threshold velocity is $\tilde{v}_0 = 0$.

To discuss the efficiency of the I-OUIS model, we additionally need to take into account the active power due to the self-propulsion velocity because $\langle \dot{u} \rangle$ is non-zero. Such a contribution can be estimated by $\dot{W}_u = \sum_i (\beta_i M / \tau_a) \langle u \rangle_i^2 p_i / T_i^*$, where $T_i^* / T = 1 + \tilde{A} / (1 + \tilde{\tau}_a / \beta_i)$ ($i = 1, 2$) [see Eq. (9)]. Using these quantities, we consider the following modified efficiency for the I-OUIS model

$$\eta_{\text{int}} = \frac{\dot{\sigma}_v}{\dot{I} + \dot{W}_u} = \frac{\sum_i \langle \tilde{v} - \tilde{u} \rangle_i \langle \tilde{v} \rangle_i p_i / \tilde{T}_i^*}{(I / \tilde{\tau}_m) + \sum_i (\beta_i / \tilde{\tau}_a) \langle \tilde{u} \rangle_i^2 p_i / \tilde{T}_i^*}, \quad (17)$$

where $\tilde{T}_i^* = T_i^* / T$. This efficiency η_{int} is plotted as a function of the measurement time $\tilde{\tau}_m$ in Fig. 2(c) when $\tilde{v}_0 = 0$. In the case of $(\beta_1, \beta_2) = (10, 1)$, for example, the efficiency takes a maximum value $\eta_{\text{int}} \approx 0.23$ at around $\tilde{\tau}_m \approx 1.43$. When β_2 is decreased to $(\beta_1, \beta_2) = (10, 0.01)$, the efficiency increases significantly up to $\eta_{\text{int}} \approx 0.72$, and it decays slowly even for large $\tilde{\tau}_m$ values.

If we do not include \dot{W}_u in the denominator of η_{int} in

Eq. (17) and simply estimate η_{ext} in Eq. (10), the latter can exceed unity for certain choices of the model parameters. A similar situation was reported for an information engine in a non-equilibrium bath [29] that shows an efficiency larger than unity [30] (called pseudo-efficiency [31]). To be consistent with the extended second law of thermodynamics with information [18], it is necessary to consider the active power \dot{W}_u resulting from the self-propulsion velocity. In Fig. S5, we have performed the simulation of the I-OUIS model with other choices of parameters for which we have fixed $(\beta_1, \tilde{\tau}_m) = (1, 0.01)$ and systematically changed β_2 . The overall behavior is robust to the choice of the parameters as long as τ_a and \tilde{A} are fixed.

So far, the strength of active (non-thermal) fluctuation in Eq. (14) has been fixed to $\tilde{A} = 1$. Choosing $(\beta_1, \beta_2, \tilde{\tau}_m) = (10, 0.1, 0.01)$ as before, we plot in Fig. 3 the velocity distribution function $P(\tilde{v})$, the average velocity $\langle \tilde{v} \rangle$, and the efficiency η_{int} of the I-OUIS model when \tilde{A} is varied from 0.1

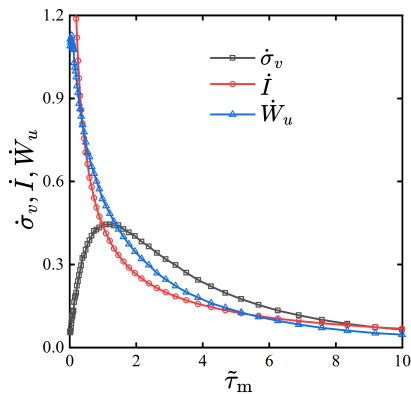


FIG. 4. Contributions of dimensionless $\dot{\sigma}_v$, \dot{I} , and \dot{W}_u to the efficiency η_{int} of the I-OUIS model [see Eq. (17)] as a function of $\tilde{\tau}_m$. The choice of parameters corresponds to that of $\tilde{A} = 10$ (purple) in Fig. 3(c).

to 10. Generally, $\langle \tilde{v} \rangle$ becomes larger and the range of \tilde{v}_0 that gives finite $\langle \tilde{v} \rangle$ becomes wider as \tilde{A} is increased. For example, the maximum velocity exceeds $\langle \tilde{v} \rangle \approx 7$ and the maximum efficiency can be as large as $\eta_{\text{int}} \approx 0.7$ when $\tilde{A} = 10$. For the E-OUIS model, however, the velocity and the efficiency cannot be so large even if the active noise is increased. Hence, the strength of active fluctuation has a significant effect on the performance of the I-OUIS, and it can also control the swimming efficiency. This is the main difference between the E-OUIS and I-OUIS models.

To discuss the efficiency η_{int} of the I-OUIS model more quantitatively, we separately plot dimensionless $\dot{\sigma}_v$, \dot{I} , and \dot{W}_u in Fig. 4 as a function of $\tilde{\tau}_m$ when $\tilde{A} = 10$ [corresponding to the purple data in Fig. 3(c)]. For small $\tilde{\tau}_m$, \dot{I} is larger than \dot{W}_u , whereas \dot{W}_u becomes larger when $\tilde{\tau}_m > 0.5$. However, \dot{I} becomes larger again than \dot{W}_u for large $\tilde{\tau}_m$ values. The contribution of $\dot{\sigma}_v$ takes a maximum value at around $\tilde{\tau}_m \approx 1$. As a result, the efficiency takes a maximum value $\eta_{\text{int}} \approx 0.74$ at around $\tilde{\tau}_m \approx 3.6$ as shown in Fig. 3(c) (the purple data). A similar behavior can also be seen for $\tilde{A} = 1$ and 5, as presented in Figs. S6(a) and (b), respectively. From these results, we find that the contribution of \dot{W}_u becomes larger as \tilde{A} is increased.

For both E-OUIS and I-OUIS models, we have considered that the measurement and feedback control cause no energy dissipation, and these swimmers acquire net locomotion without any external energy input. On the other hand, the memory spaces of these OUISs are assumed to be sufficiently large so that the information entropy stored in the memory can increase monotonically. Owing to the latter assumption, the second law of thermodynamics is not violated even though the two OUIS models can achieve a steady-state velocity under noisy conditions that are both thermal and non-thermal. For the I-OUIS model, the second law can be stated as $\eta_{\text{int}} \leq 1$ or $\dot{\sigma}_v - \dot{W}_u \leq \dot{I}$ which is equivalent to that discussed in the context of information thermodynamics [18]. Notice that the

average active power \dot{W}_u vanishes in the E-OUIS model. We emphasize again that the maximum efficiency can be obtained by tuning the measurement time τ_m for both OUIS models.

Here, we give some numbers for the model parameters. Recently, the run-and-tumble motion of *E. coli* has been quantitatively measured by using intermediate scattering functions and the renewal theory [22, 23]. For a wild-type *E. coli*, the running and tumbling times were estimated to be $\tau_R = 2.39$ s and $\tau_T = 0.38$ s, respectively, and the average self-propulsion velocity was $u_0 = 15.95 \mu\text{m/s}$. If we identify τ_a in our OUIS models, the strength of active fluctuation can be estimated as $A \approx 4 \times 10^{-10} \text{ m}^2/\text{s}$. Since the ratio β_1/β_2 can also be estimated from the ratio $\tau_R/\tau_T \approx 6$, the choice $(\beta_1, \beta_2) = (10, 1)$ in Fig. 2 is realistic for a wild-type *E. coli*. Experimentally, the running and tumbling times can be controlled by adding a chemical inducer [22, 23].

Finally, we mention that a Brownian inchworm model of a self-propelled elastic dimer was proposed before by Kumar *et. al.* [32, 33]. In their model, the crucial mechanism was to take into account the position-dependent friction coefficients of the two particles. Although such a mechanism was not regarded as an explicit feedback control operation, the proposed Brownian inchworm model offers a typical example of informational active matter [13]. Currently, we are constructing a general framework of information swimmers using the statistical formulation of Onsager-Machlup variational principle [34].

Summary.— In this Letter, we have performed numerical simulations of the information swimmers based on the active Ornstein-Uhlenbeck model; E-OUIS with external feedback control and I-OUIS with internal feedback control. Both OUIS models exhibit finite average velocities in the steady state, and their statistical properties including the efficiencies have been discussed. For both of the models, maximum efficiency can be obtained by tuning the measurement time and information entropy plays an essential role in the locomotion of the OUISs. Depending on the choice of the model parameters, I-OUIS can achieve a larger average velocity and higher efficiency than those of E-OUIS. Our models provide an important step toward understanding the directional transport in biological systems.

Acknowledgments.— We thank Y. Hosaka for the useful discussion. Z.H. and S.K. acknowledge the support by the National Natural Science Foundation of China (Nos. 12104453, 12274098, and 12250710127). S.K. acknowledges the startup grant of Wenzhou Institute, University of Chinese Academy of Sciences (No. WIUCASQD2021041). K.Y. and S.K. acknowledge the support by the Japan Society for the Promotion of Science (JSPS) Core-to-Core Program “Advanced core-to-core network for the physics of self-organizing active matter” (No. JPJSCCA20230002). K.Y. was supported in part by the Research Institute for Mathematical Sciences, an International Joint Usage/Research Center located at Kyoto University. Z.H. and Z.Z. contributed equally to this work.

-
- [1] M. C. Marchetti, J. F. Joanny, S. Ramaswamy, T. B. Liverpool, J. Prost, M. Rao, and R. A. Simha, Hydrodynamics of soft active matter, *Rev. Mod. Phys.* 85, 1143 (2013).
- [2] Y. Hosaka and S. Komura, Nonequilibrium transport induced by biological nanomachines, *Biophys. Rev. Lett.* 17, 51 (2022).
- [3] P. Romanczuk, M. Bär, W. Ebeling, B. Lindner, and L. Schimansky-Geier, Active Brownian particles, *Eur. Phys. J.: Spec. Top.* 202, 1 (2012).
- [4] G. E. Uhlenbeck and L. S. Ornstein, On the theory of the Brownian motion, *Phys. Rev.* 36, 823 (1930).
- [5] D. Martin, J. O'Byrne, M. E. Cates, É. Fodor, C. Nardini, J. Tailleur, and F. van Wijland, Statistical mechanics of active Ornstein-Uhlenbeck particle, *Phys. Rev. E* 103, 032607 (2021).
- [6] B. ten Hagen, S. van Teeffelen, and H. Löwen, Brownian motion of a self-propelled particle, *J. Phys.: Condens. Matter* 23, 194119 (2011).
- [7] A. Najafi and R. Golestanian, Simple swimmer at low Reynolds number: Three linked spheres, *Phys. Rev. E* 69, 062901 (2004).
- [8] K. Yasuda, Y. Hosaka, and S. Komura, Generalized three-sphere microswimmers, *J. Phys. Soc. Jpn.* 92, 121008 (2023).
- [9] R. Golestanian and A. Ajdari, Analytic results for the three-sphere swimmer at low Reynolds number, *Phys. Rev. E* 77, 036308 (2008).
- [10] J. R. Howse, R. A. L. Jones, A. J. Ryan, T. Gough, R. Vafabakhsh, and R. Golestanian, Self-Motile Colloidal Particles: From Directed Propulsion to Random Walk, *Phys. Rev. Lett.* 99, 048102 (2007).
- [11] K. Yasuda, Y. Hosaka, I. Sou, and S. Komura, Odd microswimmer, *J. Phys. Soc. Jpn.* 90, 075001 (2021).
- [12] J. Li, Z. Zhang, Z. Hou, K. Yasuda, and S. Komura, Time-correlation functions of stochastic three-sphere micromachines, *Phys. Rev. E* 110, 044603 (2024).
- [13] B. VanSaders and V. Vitelli, Informational active matter, *arXiv:2302.07402*.
- [14] S. Toyabe, T. Sagawa, M. Ueda, E. Muneyuki, and M. Sano, Experimental demonstration of information-to-energy conversion and validation of the generalized Jarzynski equality, *Nat. Phys.* 6, 988 (2010).
- [15] G. Paneru, S. Dutta, T. Sagawa, T. Thlusty, and H. K. Pak, Efficiency fluctuations and noise induced refrigerator-to-heater transition in information engines, *Nat. Commun.* 11, 1012 (2020).
- [16] G. Paneru, S. Dutta, and H. K. Pak, Colossal power extraction from active cyclic Brownian information engines, *J. Phys. Chem. Lett.* 13, 6912 (2022).
- [17] C. Huang, M. Ding, and X. Xing, Information swimmer: Self-propulsion without energy dissipation, *Phys. Rev. Res.* 2, 043222 (2020).
- [18] J. M. R. Parrondo, J. M. Horowitz, and T. Sagawa, Thermodynamics of information, *Nat. Phys.* 11, 131 (2015).
- [19] V. Serreli, C.-F. Lee, E. R. Kay, and D. A. Leigh, A molecular information ratchet, *Nature (London)* 445, 523 (2007).
- [20] W. Hwang and M. Karplus, Structural basis for power stroke vs. Brownian ratchet mechanisms of motor proteins, *Proc. Natl. Acad. Sci. U.S.A.* 116, 19777 (2019).
- [21] G. Tkačik and W. Bialek, Information processing in living systems, *Annu. Rev. Condens. Matter Phys.* 7, 89 (2016).
- [22] C. Kurzthaler, Y. Zhao, N. Zhou, J. Schwarz-Linek, C. Devailly, J. Arlt, J.-D. Huang, W. C. K. Poon, T. Franosch, J. Tailleur, and V. A. Martinez, Characterization and control of the run-and-tumble dynamics of *Escherichia Coli*, *Phys. Rev. Lett.* 132, 038302 (2024).
- [23] Y. Zhao, C. Kurzthaler, N. Zhou, J. Schwarz-Linek, C. Devailly, J. Arlt, J.-D. Huang, W. C. K. Poon, T. Franosch, V. A. Martinez, and J. Tailleur, Quantitative characterization of run-and-tumble statistics in bulk bacterial suspensions, *Phys. Rev. E* 109, 014612 (2024).
- [24] L. Caprini and U. M. B. Marconi, Inertial self-propelled particles, *J. Chem. Phys.* 154, 024902 (2021).
- [25] G. H. P. Nguyen, R. Wittmann, and H. Löwen, Active Ornstein-Uhlenbeck model for self-propelled particles with inertia, *J. Phys. Condens. Matter* 34, 035101 (2022).
- [26] R. García-García, P. Collet, and L. Truskinovsky, Guided active particles, *Phys. Rev. E* 100, 042608 (2019).
- [27] M. Doi, *Soft Matter Physics* (Oxford University Press, Oxford, 2013).
- [28] P. E. Kloeden and E. Platen, Numerical Solution of Stochastic Differential Equations (Springer, Berlin, 1992).
- [29] R. Di Leonardo, L. Angelani, D. Dell'Arciprete, G. Ruocco, V. Iebba, S. Schippa, M. P. Conte, F. Mecarini, F. De Angelis, and E. Di Fabrizio, Bacterial ratchet motors, *Proc. Natl. Acad. Sci. U.S.A.* 107, 9541 (2010).
- [30] T. K. Saha, J. Ehrich, M. Gavrilov, S. Still, D. A. Sivak, and J. Bechhoefer, Information engine in a nonequilibrium bath, *Phys. Rev. Lett.* 131, 057101 (2023).
- [31] A. Datta, P. Pietzonka, and A. C. Barato, Second law for active heat engines, *Phys. Rev. X* 12, 031034 (2022).
- [32] K. V. Kumar, S. Ramaswamy, and M. Rao, Active elastic dimers: Self-propulsion and current reversal on a featureless track, *Phys. Rev. E* 77, 020102(R) (2008).
- [33] A. Baule, K. V. Kumar, and S. Ramaswamy, Exact solution of a Brownian inchworm model for self-propulsion, *J. Stat. Mech.*, P11008 (2008).
- [34] K. Yasuda, K. Ishimoto, and S. Komura, Statistical formulation of Onsager-Machlup variational principle, *Phys. Rev. E* 110, 044104 (2024).